A&A 505, 541–551 (2009)
DOI: 10.1051/0004-6361/200911687

Astronomy & Astrophysics

Characterization of the emitting and absorbing media around the nucleus of the active galaxy UGC 11763 using XMM-Newton data

M. V. Cardaci[1,2], M. Santos-Lleó[2], Y. Krongold[3], G. F. Hägele[1,4], A. I. Díaz[1], and P. Rodríguez-Pascual[2]

[1] Universidad Autónoma de Madrid, Ctra. de Colmenar Km.15, Cantoblanco, 28049 Madrid, Spain
[2] XMM-Newton Science Operations Center, ESAC, ESA, POB 78, 28691 Villanueva de la Cañada, Madrid, Spain
e-mail: Monica.Cardaci@sciops.esa.int
[3] Instituto de Astronomía, Universidad Nacional Autónoma de México, Apartado Postal 70-264, 04510 México DF, México
[4] Facultad de Cs. Astronómicas y Geofísicas, Universidad Nacional de La Plata, Paseo del Bosque s/n, 1900 La Plata, Argentina

Received 20 January 2009 / Accepted 11 July 2009

ABSTRACT

Aims. The detailed analysis of all data taken by the *XMM-Newton* satellite of UGC 11763 to characterize the different components that are emitting and absorbing radiation in the vicinity of the active nucleus.
Methods. The continuum emission was studied through the EPIC spectra taking profit of the spectral range of these cameras. The high resolution RGS spectra were analyzed in order to characterize the absorbing features and the emission line features that arise in the spectra of this source.
Results. A power law with a photon index $\Gamma = 1.72^{+0.03}_{-0.01}$ accounts for the continuum emission of this source in the hard X-rays from 10 down to 1 keV. At lower energies, a black body model with $kT = 0.100 \pm 0.003$ keV provides a good description of the observed soft excess. The absorption signatures in the spectra of UGC 11763 are consistent with the presence of a two phase ionized material ($\log U = 1.65^{+0.07}_{-0.08}$; 2.6 ± 0.1 and $\log N_{\rm H} = 21.2 \pm 0.2$; 21.51 ± 0.01 cm^{-2}, respectively) in the line of sight. The physical conditions found are consistent with the two phases being in pressure equilibrium. The low ionization component is more ionized than typically found for warm absorbers in other Seyfert 1 galaxies. There are also signatures of some emission lines: OVII Heα(r), OVII Heα(f), a blend of the NeIX Heα triplet and FeXVIII at λ 17.5 Å.

Key words. galaxies: active – galaxies: Seyfert – galaxies: individual: UGC 11763 – X-rays: galaxies

1. Introduction

Narrow Line Seyfert 1 (NLS1) galaxies are active galactic nuclei that share many properties with Seyfert 1 galaxies, such as a strong continuum and strong FeII emission lines, but whose line widths are similar to those of Seyfert 2 galaxies (Osterbrock & Pogge 1985). The more striking characteristics of these objects concern their X-ray spectra, that show strong soft excess emission (Boller et al. 1996), a rapid and large-amplitude variability (Boller 2000), and generally a steeper hard X-ray continua than "normal" Seyfert 1 objects (Brandt et al. 1997). Different models have been suggested to describe the nature of these objects (Ghosh et al. 2004) and the most accepted paradigm is that NLS1s possess low mass black holes (about 10^7 $M_\odot$) that are accreting material close to the Eddington rate (Boroson 2002; Grupe & Mathur 2004).

Photoionized X-ray absorbing gas is observed associated with a good number of NLS1 galaxies (see e.g. Komossa 2000, and references therein). This highly ionized material, called "warm absorber", has also been detected in about 50% of type 1 Active Galactic Nuclei (AGNs), both Seyfert 1s (Halpern 1982; Reynolds 1997; George et al. 1998) and quasars (Piconcelli et al. 2005). Crenshaw et al. (1999) and Kriss (2002) found that all the objects in their sample that exhibit signatures of X-ray warm absorbers also show intrinsic ultra-violet (UV) absorption. In some cases there is evidence suggesting that the same medium is responsible for the absorptions in both X-rays and UV (e.g. Mathur et al. 1994, 1995; Kriss et al. 2000). In others, however, this correspondence is not so clear. In NGC 7469 (Kriss et al. 2003) and NGC 3783 (Gabel et al. 2003) it was found that some of the UV absorbing components could be related with the X-ray absorbing ones. On the other hand, in NGC 4051, e.g., the physical conditions found for both absorbing components were different (Steenbrugge et al. 2009). Perhaps due to the complexity of the physics of the absorbing media the exact relation between the X-ray and UV absorbing systems is still unclear.

UGC 11763, also known as II Zw 136, Mrk 1513 or PG 2130+099, among other names, has been classified as a NLS1 galaxy by Constantin & Shields (2003). The width of the Hβ line in this object is between 2250–2800 km s^{-1} (Boroson & Green 1992; Grupe et al. 2004; Mullaney & Ward 2008; Grier et al. 2008), only slightly above the upper limit for the NLS1 classification. It was included in the NLS1 sample of Boroson & Green (1992) and Gallo (2006) although Boller et al. (1996) excluded it from their list. On the other hand, Véron-Cetty & Véron (2006) have classified it as an intermediate Seyfert (Seyfert 1.5). Huchra et al. (1999) estimated an optical redshift $z = 0.062977$ for this object whose position coordinates are $\alpha_{2000} = 21^{\rm h}32^{\rm m}27\overset{\rm s}{.}81$, $\delta_{2000} = +10°08'19''.46$ (Clements 1981).

UGC 11763 has been studied over a wide range of wavelengths. Using optical spectra Mullaney & Ward (2008) fitted the two strongest Balmer Hydrogen lines with three emission line components, the widest of them (FWHM of about 4500

and 5100 km s^{-1} for Hα and Hβ, respectively) being typical of the broad lines found in 'normal' Seyfert 1 galaxies, i.e. ~3000 km s^{-1}. Besides, they also estimated the widths of a broad component in the [Fe VII] λ 6087 Å and [Fe X] λ 6374 Å lines (~2000 and ~2700 km s^{-1}, respectively) which turned out to be very similar to the intermediate width component of the Balmer lines (~2100 and 2350 km s^{-1} for Hα and Hβ, respectively). For the central black hole mass, Peterson et al. (2004) derived a value of $4.57 \pm 0.55 \times 10^8$ $M_\odot$. Ho et al. (2008) reduced this value by a factor of 1.8 (2.5×10^8 $M_\odot$) for consistency with the virial mass zero point adopted by Greene & Ho (2005). This value is in the upper limit of the NLS1 black hole mass distribution found by Grupe & Mathur (2004). Nevertheless, it has been further reduced to $3.8 \pm 1.5 \times 10^7$ $M_\odot$ by Grier et al. (2008) more in the range of what is observed in this kind of objects.

In X-rays, it was observed by *EXOSAT*, *Einstein*, *Ginga* and *ROSAT* satellites. Singh et al. (1991) analyzed *EXOSAT* data to investigate the variability and the soft excess in the X-ray spectrum. They found that in one year the X-ray flux varies by ~35% in the 1.5–6 keV band and by a factor of ~2 in the low energy range (0.1–2 keV). They also reported that the low-energy component is very steep ($\Gamma \approx 6$) and dominates the spectrum below 0.5 keV, irrespective of whether the object is in a high or low state. A soft excess was also found by Masnou et al. (1992) using *Einstein Imaging Proportional Counter*, covering the energy range ~0.15–3.5 keV.

Williams et al. (1992) reported spectra in the 2–20 keV range from *Ginga*, and Lawson & Turner (1997), using the same observations, derived the parameters of the Fe Kα emission line at 6.4 keV. Recently, Inoue et al. (2007) studied the EPIC-pn data from *XMM-Newton* satellite as part of a wider Fe Kα line studio. These authors found that this line is narrow ($\sigma = 0.02^{+0.22}_{-0.02}$ keV) and has an equivalent width (*EW*) of 139^{+495}_{-139} eV.

Regarding the AGN surrounding medium, extreme UV observations with FUSE have shown absorption features due to H (Lyα to Lyζ), CIII λ 977 Å and OVI $\lambda\lambda$ 1032,1038 Å originated in an associated system (Wakker et al. 2003) whose relative velocity with respect to the AGN (–1600 km s^{-1}) does not allow to rule out that this absorption system be associated with UGC 11763, rather than an intergalactic cloud. Dunn et al. (2007), using the same and newer observations from FUSE, also found this blue shifted component, with a velocity of −1500 km s^{-1}, together with a second one of 20 km s^{-1}, both relative to the AGN. According to these authors, the former component is clearly visible and virtually free of ISM interference, while the latter one is only appreciable in the OVI red member, the blue member of this line being contaminated with an FeII and two H_2 close lines. These two absorption components were also found by Crenshaw et al. (1999) using *GHRS-HST* (Goddard High-Resolution Spectrometer-Hubble Space Telescope) UV spectra.

In this paper we present a detailed analysis of all the available data obtained with the *XMM-Newton* satellite in order to characterize the circumnuclear environment of this NLS1 galaxy. In Sect. 2 we describe the observations and data reduction. We present the optical-UV results in Sect. 3 and the X-ray spectral analysis in Sect. 5. In Sect. 4 we analyze the source variability during the *XMM-Newton* observation and compare our observed fluxes with those from the literature. Our results are discussed in Sect. 6. Finally, the summary and conclusions of this work are given in Sect. 7.

Table 1. Details of *XMM-Newton* instrument exposures.

Instrument	Mode	Filter	Time (s) Scheduled	Time (s) Effective
EPIC-pn	Small Window	Thin	37511	24609[a]
EPIC-MOS1	Small Window	Thick	37660	36476
EPIC-MOS2	Full Frame	Thin	37672	34114
RGS1	Spectroscopy	–	37917	36141
RGS2	Spectroscopy	–	37913	36145
OM	Image	U	1000	
OM		UVW1	2 × 1000	
OM		UVM2	2 × 1000	
OM		UVW2	2 × 1000	
OM		UV Grism	19 × 1000	

[a] The live time of the EPIC-pn small window mode is 0.71.

2. Observations

UGC 11763 was observed with *XMM-Newton* (Jansen et al. 2001) on May 16th, 2003. The complete observation, with Id. number 0150470701, lasted for 39 ks. In order to avoid potential pile-up problems, EPIC-pn and MOS1 cameras (Turner et al. 2001) were used in their small window mode with the thin and thick filters, respectively. EPIC-MOS2 was operated in full frame mode (thin filter) in order to allow investigation of other serendipitous X-ray sources in the field. The Reflection Grating Spectrometers (RGSs, den Herder et al. 2001) were run in the default Spectroscopy mode. For the Optical Monitor (OM) (Mason et al. 2001) we decided to combine broad-band imaging filters to investigate the circumnuclear structure in the UV domain with a series of UV-Grism exposures to obtain UV spectral and variability information of the active nucleus. The OM was always operated with windows defined by us: we used the largest imaging un-binned window, 5′.1 × 5′.0, centered on the target for the broad-band filters and the default grism window for the UV exposures. Table 1 lists instrument, mode, filter and scheduled exposure time for each instrument.

The data have been processed with the 7.0.0 version of the Science Analysis Subsystem (SAS) software package (Jansen et al. 2001), using the calibration files available on March, 2007. All the standard procedures and screening criteria have been followed in the extraction of the scientific products.

During most of the observing time the background count rate in the EPIC cameras was well below 10% of the source count rate. High background time intervals have been excluded using the method that maximizes the signal to noise in the spectrum as described in Piconcelli et al. (2004). Hence, the maximum count rate allowed for the background in "good" periods was 0.5 c s^{-1}, 0.5 c s^{-1} and 0.7 c s^{-1} for EPIC-pn, EPIC-MOS1 and EPIC-MOS2, respectively. For RGS1 and RGS2, periods with count rates higher than 0.2 c s^{-1} have been excluded. The last column of Table 1 lists the final exposure time after taking into account live time[1] and high background screening, per exposure.

[1] The live time is the ratio between the time interval during which the CCD is collecting X-ray events (integration time, including any time needed to shift events towards the readout) and the frame time (which in addition includes time needed for the readout of the events). XMM-Newton Users Handbook (`http://xmm.esac.esa.int/external/xmm_user_support/documentation/uhb/node28.html`).

Table 2. Fluxes in the OM filters obtained using aperture photometry.

Filter	Effective wavelength (Å)	Flux (10^{-14} erg s^{-1} cm^{-2} Å^{-1})
U	3440	1.05 ± 0.01
UVW1	2910	1.24 ± 0.01[a]
UVM2	2310	1.24 ± 0.02[a]
UVW2	2120	1.58 ± 0.05[a]

[a] Fluxes are the mean values of the two exposures on each filter.

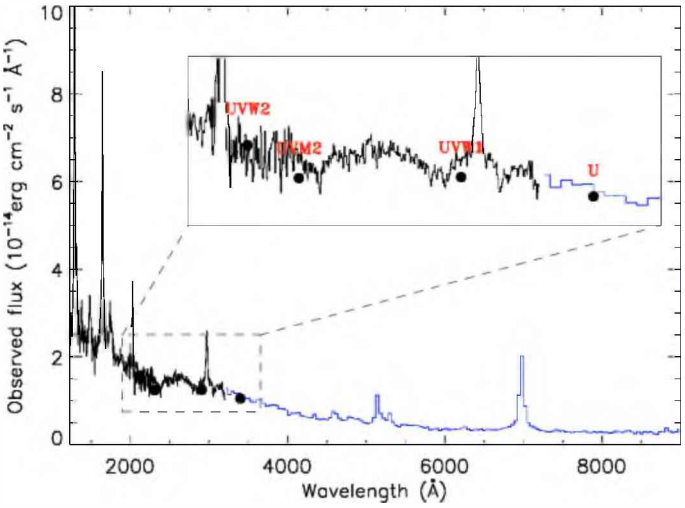

Fig. 1. Average IUE spectrum of UGC 11763 (1200–3200 Å, in black) merged with the optical spectrum (3200–9000 Å, in blue) from de Bruyn & Sargent (1978). Solid red circles show the OM measures for the different filters.

3. Optical-UV analysis

OM data have been processed with SAS task OMICHAIN and default parameters. In the broad-band OM images there is no clear evidence of extended emission. Unfortunately, the spectrum recorded in each individual UV-grism exposure is very weak; in addition, a number of zero-order images near the spectrum location and along the dispersion further complicate the extraction of the source spectrum. As a result, the total signal-to-noise of the extracted spectra was not as high as expected.

The broad-band OM images provide flux measures in the *U*, *UVW1*, *UVM2* and *UVW2* filters. For the last three bands, two consecutive exposures are available; the flux differences in these three pairs of consecutive exposures are all compatible with no variability within the measurement errors (<3%). Table 2 shows the effective wavelengths of these filters together with measured fluxes.

UGC 11763 was observed by the *International Ultraviolet Explorer* (IUE) in six different epochs between 1978 and 1985, with its Short Wavelength (1150–1950 Å) and Long Wavelength (1950–3200 Å) spectrographs. Variations of ∼25% around the mean are found along the whole IUE range, with the ratio of maximum to minimum UV flux being close to 2. OM flux measurements are overplotted in Fig. 1 on a merged spectrum constructed by combining the average IUE spectrum and the optical one presented by de Bruyn & Sargent (1978).

The difference between the OM measures and the average IUE spectrum at the effective wavelengths of the OM filters is consistent with the combined errors of the IUE average spectrum and the OM filter sensibility. Therefore, we conclude that the average UV and the optical spectra are indeed an acceptable representation of the UV-optical spectral energy distribution (SED) of UGC 11763 at the time of the *XMM-Newton* observation. From the IUE average spectrum we take the UV flux at 2500 Å, $F(2500\ \text{Å}) = 1.53 \times 10^{-14}$ erg s^{-1} cm^{-2} Å^{-1}, that we have used to compute the optical/X-ray spectral index α_{ox} (Tananbaum et al. 1979). This value has neither been corrected for the Balmer continuum nor the FeII contributions.

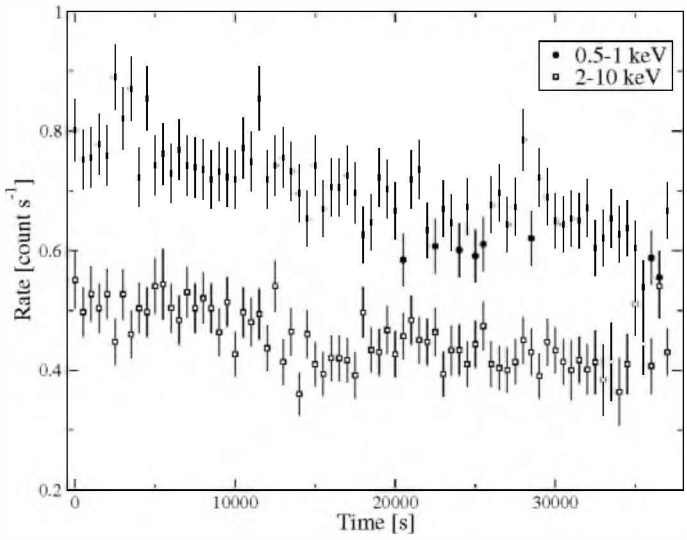

Fig. 2. Soft (filled circles) and hard (open squares) EPIC-pn light curves binned by 500 s.

4. Variability

We have analyzed the EPIC-pn soft (0.5–1 keV) and hard (2–10 keV) X-ray background subtracted light curves (Fig. 2) to investigate the variability of this source during the observation by computing the statistical validity of constant flux assumption. Values of χ^2_ν of 2.2 and 1.3 are found for the soft and hard energy bands respectively. Taking into account that a $\chi^2_\nu > 1.2$ corresponds to a probability of less than 10% and $\chi^2_\nu > 1.4$ to a probability of less than 1% for the data to be well represented by a constant flux value, this implies that the flux varied during the observation.

The overall behavior of the light curves seems to show a decrease of the flux from the beginning to the end of the observation. Applying a linear fit, we find a rate of change in the count rates of about $-5.1(\pm0.5) \times 10^{-6}$ counts s^{-2} ($\chi^2_\nu = 0.9$) and $-2.7(\pm0.5) \times 10^{-6}$ counts s^{-2} ($\chi^2_\nu = 0.8$) for the soft and hard bands, respectively. The statistic of the linear fit, with probabilities of 73 and 86% for the data to be well represented by the linear model, implies that this simple model only reproduces the general trend of the flux variation. The maximum flux decrease during the observation can be quantified by computing the ratio between the maximum and the minimum rate which is found to be $1.7^{+0.3}_{-0.2}$ and $1.5^{+0.4}_{-0.3}$ for the soft and hard X-ray bands, respectively.

We have compiled several values of X-ray fluxes published for UGC 11763 along the years (Table 3). This object was also serendipitously observed by *XMM-Newton* (EPIC-pn) during a slew on the 14th of May 2006. We have also included in Table 3 the soft and hard X-ray fluxes as provided in the XMM-Newton slew survey Source Catalogue (XMMSL1.2, Saxton et al. 2008). UGC 11763 shows a large amplitude variation in its soft X-ray flux. If we compare the flux in the 0.1–2.4 keV range obtained

Table 3. Comparison between X-ray fluxes from the literature and from this work.

Data	Obs. date	Flux			Ref.
		Soft		Hard	
		0.1–2 keV	0.1–2.4 keV	2–10 keV	
EXOSAT	1984 Nov.	4.2	–	5.6	1
EXOSAT	1985 Nov.	9.5	–	6.3	1
GINGA	1989 Nov.	–	–	4.7	2
ROSAT	1990 Nov.	–	33.1	–	3
XMM	2003 May	–	–	3.63	4
XMM	2003 May	$2.70^{+0.19}_{-0.08}$	3.00 ± 0.08	$3.65^{+0.07}_{-0.08}$	5
XMM	2006 May	16 ± 2^a	–	10 ± 3^b	6

Fluxes are given in 10^{-12} erg s^{-1} cm^{-2}. [a] Flux between 0.2–2 keV. [b] Flux between 2–12 keV. References: (1) Singh et al. (1991); (2) Williams et al. (1992); (3) Voges et al. (1999); (4) Inoue et al. (2007); (5) this work; (6) XMM-Newton slew survey Source Catalogue (Saxton et al. 2008).

from the *ROSAT* observation with our measurement we find about an order of magnitude variation between these two epochs. The 2006 data of the slew observation show that UGC 11763 had returned to flux values similar to those of 1990. In the 2–10 keV range the amplitude of the flux variation is higher than a factor of 2. Unfortunately, there is no data in the hard spectral range corresponding to the observed highest soft X-ray flux. Taking into account the fluxes in Table 3 for this object, it becomes clear that, in 2003, *XMM-Newton* observed it in the lowest activity state so far reported.

5. X-ray spectral analysis

All the EPIC data were checked for no pile-up using the SAS task EPATPLOT. The coordinates of the center of the EPIC-pn X-ray source are within 1″ of the optical coordinates of UGC 11763 quoted in Sect. 1. The EPIC spectra were extracted using the standard parameters. For the EPIC-pn spectrum the source extraction area was a circular region of 32.′5 in radius. The background extraction area was a circular region at 2.′0 North-NW of the target and of 32.′5 in radius. The EPIC-MOS1 source spectrum was extracted using a circular region of 40″ radius. The background region was an annulus centered in the source with 8′ and 9.′2 inner and outer radius, respectively. The EPIC-MOS2 source spectrum was extracted using a circular region with 1′ radius and the background was extracted from an annular region also centered in the target position and 2.′5 and 3.′6 inner and outer radius, respectively. The three EPIC spectra have been rebinned to have at least 30 counts per bin and a maximum of three channels per resolution (FWHM) element of the detector.

The RGS data has been processed with the SAS task RGSPROC and default parameters, except that we asked for the background subtracted spectra. In spite of UGC 11763 being a bright object when observed by *ROSAT* (Voges et al. 1999), it seems to be in a lower state when observed by *XMM-Newton* satellite (see discussion in Sect. 4). As a result, the scheduled time for the *XMM-Newton* observation does not allow to achieve as good signal-to-noise in the RGS spectra as expected. We therefore had to bin the spectra, loosing resolution, but increasing the signal-to-noise ratio. The RGS spectra were geometrically binned to avoid any smoothing of the absorption and emission features. We chose a 15 channels binning as a compromise between loosing resolution and having the necessary spectral signal-to-noise for a statistically significant fit. Hence, as the default spectral bin size is 10 mÅ, at 15 Å, our final spectra have bins of about 150 mÅ at that wavelength.

Table 4. EPIC-pn fit model parameters for the 2–10 keV energy range.

Model component	Parameter	Value
powerlaw	Γ	$1.65^{+0.06}_{-0.05}$
	$K_{\rm pwlw}$	$8.3^{+0.6}_{-0.6}$
statistic	χ^2_ν	1.07
	d.o.f.	112
powerlaw	Γ	$1.69^{+0.06}_{-0.06}$
	$K_{\rm pwlw}$	$8.6^{+0.4}_{-0.3}$
Gaussian	$E_{\rm rest}$	$6.35^{+0.16}_{-0.34}$
	σ	$0.26^{+0.52}_{-0.11}$
	$K_{\rm line}$	$0.9^{+1.1}_{-0.5}$
statistic	χ^2_ν	0.99
	d.o.f.	109

The galactic $N_{\rm H}$ is fixed to 4.67×10^{20} cm^{-2}. The line energy in the rest frame of the source ($E_{\rm rest}$) and σ of the Fe-Kα emission line are given in keV; power-law normalizations ($K_{\rm pwlw}$) in units of 10^{-4} ph keV^{-1} cm^{-2} s^{-1} at 1 keV; and line normalization $K_{\rm line}$ in units of 10^{-5} ph cm^{-2} s^{-1}. Errors quoted are at 90% confidence level.

All spectra have been fitted using *Sherpa* package of *CIAO 3.3* (Freeman et al. 2001). We use the χ^2 statistics with the Gehrels variance function (Gehrels 1986) and the Powell optimization method. The first because it is based on Poisson statistics for small number of counts in a bin and on Binomial statistics otherwise, and the second because is a robust direction-set method for finding the nearby fit-statistic minimum.

5.1. Low resolution spectra

An absorbed power law has been fitted to the EPIC-pn spectrum in the 2.0–10.0 keV energy range. The H column density has been fixed to the Galactic value of $N_{\rm H} = 4.67 \times 10^{20}$ cm^{-2} (Dickey & Lockman 1990). The result (see Table 4) has a reduced χ^2 of $\chi^2_\nu = 1.07$ for 112 degrees of freedom (d.o.f.). Adding a redshifted Gaussian emission line at the energy of the neutral Fe-Kα fluorescence line does improve the fit (Table 4), with a new value of $\chi^2_\nu = 0.99$ for 109 d.o.f. ($F = 4.1$, probability 99.19%). The line is weak with an equivalent width of $0.23^{+0.15}_{-0.11}$ keV. The model parameter values are listed in Table 4 and the fit is shown in Fig. 3. Leaving the absorbing column density as a free parameter the neutral H column density takes a value lower than the Galactic one, indicating that a neutral absorber, either local or at the UGC 11763 redshift, does not improve the fit. Hence, unless otherwise specified, all the models mentioned from here on include neutral absorption by the Galaxy with the column density fixed to above value. When the 1.0–2.0 keV range is included in the fit (i.e. a 1.0–10.0 keV EPIC-pn fit is performed), the results do not change significantly indicating little or no effects of any other component in this energy range.

Plotting the 2–10 keV energy range model overlapped to the whole 0.35–10 keV energy range (Fig. 4) it becomes clear that the flux below 1 keV exceeds the extrapolation of the harder power law flux. This is a frequent feature of AGN X-ray spectra and usually referred to as the soft X-ray excess. Typical models used to fit the soft excess are one or several black bodies,

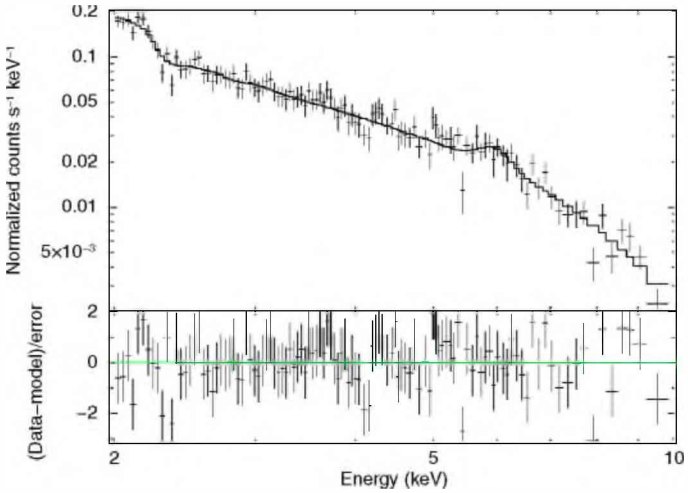

Fig. 3. EPIC-pn spectrum of the UGC 11763 nucleus, showing the power law fit to the 2–10 keV range. Galactic absorption and a neutral Fe-Kα fluorescence line are also included in the fit. (See Table 4 for the best fitting parameters.)

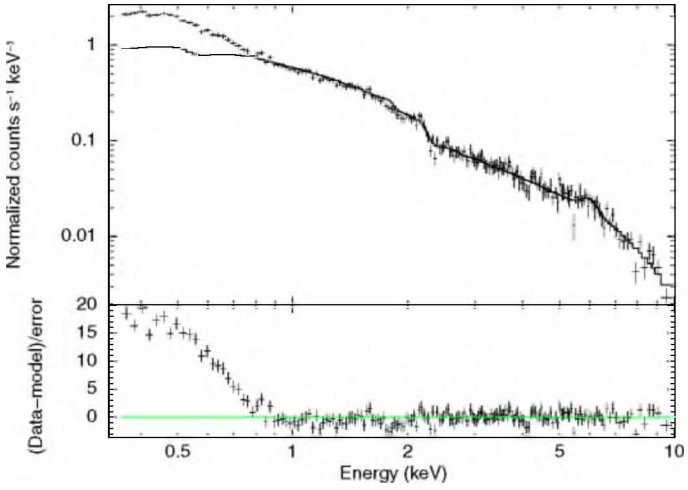

Fig. 4. EPIC-pn spectrum of the UGC 11763 nucleus, showing the whole, 0.35–10 keV energy range and the fit to the 2–10 keV range. The fit has two components, a power law and a Gaussian emission line at 6.36 keV, absorbed by the Galactic column density. A huge soft excess below ~0.9 keV is clearly shown in the residuals panel.

Table 5. Model $\mathcal{A}$ parameters for the simultaneous EPIC-pn, EPIC-MOS1 and EPIC-MOS2 spectrum fit in the 0.35–10 keV energy range.

Model component	Parameter	Value
powerlaw	Γ	1.63 ± 0.02
	$K_{\rm pwlw}$	7.9 ± 0.2
Gaussian	$E_{\rm rest}$	$6.36^{+0.15}_{-0.27}$
	σ	$0.34^{+0.33}_{-0.15}$
	$K_{\rm line}$	$1.0^{+0.6}_{-0.4}$
black body	kT	0.090 ± 0.002
	$K_{\rm bb}$	3.2 ± 0.2
statistic	χ^2_ν	0.97
	d.o.f.	509

The galactic $N_{\rm H}$ is fixed to 4.67×10^{20} cm^{-2}. The line energy is given in the rest frame of the source. The normalizations $K_{\rm pwlw}$ and $K_{\rm bb}$ correspond to the EPIC-pn spectrum. $E_{\rm rest}$, σ and kT in keV, $K_{\rm pwlw}$ in 10^{-4} ph keV^{-1} cm^{-2} s^{-1} at 1 keV, $K_{\rm line}$ in 10^{-5} ph cm^{-2} s^{-1}, and $K_{\rm bb}$ in units of 10^{-5} L_{39}/D^2_{10} where L_{39} is the source luminosity in units of 10^{39} erg s^{-1} and D_{10} is the distance to the source in units of 10 kpc. Errors quoted are at 90% confidence level.

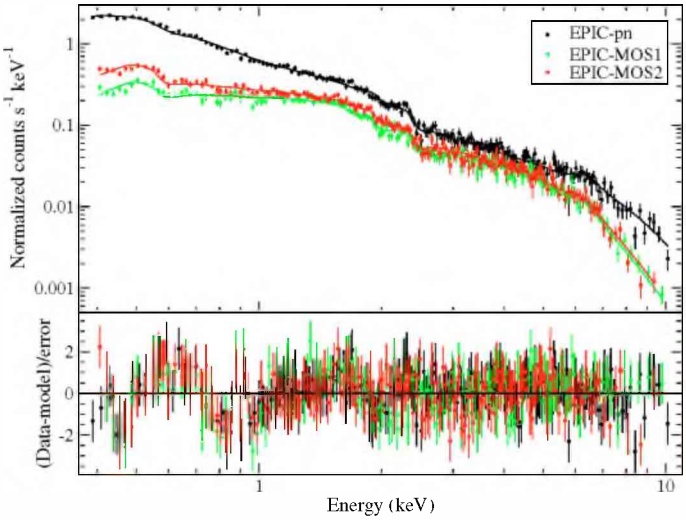

Fig. 5. EPIC-pn, EPIC-MOS1 and EPIC-MOS2 spectra – in the rest frame – of the UGC 11763 nucleus, showing the best fit model $\mathcal{A}$ (Table 5). The model includes Galactic absorption plus a power law, a black body and the Fe-Kα line. Residuals between 0.7 and 0.8 keV are clearly seen in the lower panel consistent with the presence of absorption by ionized material. See text for more details.

bremsstrahlung radiation or a higher photon index power law (e.g. Piconcelli et al. 2005). Using these models to describe the three UGC 11763 EPIC spectra in the 0.35 to 10 keV range, we find that a model with a black body component (hereafter model $\mathcal{A}$) with $kT = 0.09$ keV provides the best description of the soft excess observed in this object (Table 5). Nevertheless, although the overall fit is good ($\chi^2_\nu = 0.97$ for 509 d.o.f.), there are large residuals at low energies (see Fig. 5). They are largest around 0.7–0.8 keV or 16–17 Å, where a blend of several iron inner M-shell absorption lines, known as the Fe "Unresolved Transition Array" (UTA), has been detected in other Seyfert 1 galaxies and interpreted as the signature of ionized gas in the line of sight to the X-ray source (e.g. Sako et al. 2001). There are also large residuals around 0.5–0.6 keV where some oxygen emission lines could be present (O VII $\lambda\lambda$ 21.6, 21.8, 22.1 Å).

5.2. High resolution X-ray spectra

The better resolution of the RGS spectra as compared to the EPIC spectra favors the identification and fitting of the absorption and narrow emission features. Hence, in order to take advantage of the whole information acquired by *XMM-Newton* we use simultaneously the EPIC-pn, the two EPIC-MOS and the two high resolution RGS spectra. EPIC-pn and EPIC-MOS data are restricted from 0.35 to 10 keV, and RGS data are taken between 0.41 and 1.8 keV.

The residuals of the EPIC fit from model $\mathcal{A}$ seem to disclose the presence of partially ionized absorbing material in the line of sight to the source. The signature of this warm material, a characteristic Fe unresolved transition array (UTA), is clearly seen on the high resolution RGS spectra.

Table 6. PHASE and continuum parameter values for models $\mathcal{B}$ and C for the simultaneous fits to the EPIC and RGS spectra.

	Powerlaw		Black body		LIC			HIC			χ^2_ν/d.o.f.
	Γ	$K_{\rm pwlw}$	kT	$K_{\rm bb}$	log U	log $N_{\rm H}$	vel.	log U	log $N_{\rm H}$	vel.	
model $\mathcal{B}$	$1.67^{+0.03}_{-0.02}$	$8.3^{+0.3}_{-0.2}$	$0.097^{+0.003}_{-0.003}$	$3.4^{+0.2}_{-0.2}$	$1.7^{+0.4}_{-0.1}$	$21.0^{+0.2}_{-0.2}$	-300^{+300}_{-300}				0.97/719
model C	$1.72^{+0.03}_{-0.01}$	$8.9^{+0.3}_{-0.3}$	$0.100^{+0.003}_{-0.003}$	$3.4^{+0.2}_{-0.3}$	$1.65^{+0.07}_{-0.08}$	$21.2^{+0.2}_{-0.2}$	500^{+300}_{-300}	$2.6^{+0.1}_{-0.1}$	$21.51^{+0.01}_{-0.01}$	500^{+300}_{-300}	0.90/706

Model $\mathcal{B}$ is similar to model $\mathcal{A}$ with one absorbing component and model C to model $\mathcal{B}$ with another absorbing component and a few Gaussian emission lines (see their parameters in Table 7). Both $\mathcal{B}$ and C models include the Galactic absorption (with fixed $N_{\rm H} = 4.67 \times 10^{20}$ cm^{-2}) and the Fe-Kα line (with its parameters fixed to the model $\mathcal{A}$ values). Normalizations $K_{\rm pwlw}$ and $K_{\rm bb}$ correspond to the EPIC-pn spectrum. $K_{\rm pwlw}$ in units of 10^{-4} ph keV^{-1} cm^{-2} s^{-1}; kT in keV; $K_{\rm bb}$ in $10^{-5}\, L_{39}/D^2_{10}$ where L_{39} is the source luminosity in units of 10^{39} erg s^{-1} and D_{10} is the distance to the source in units of 10 kpc. $N_{\rm H}$ is given in cm^{-2}. Velocities, given in km s^{-1}, are relative to the systemic velocity of UGC 11763. Errors quoted are at 90% confidence level.

To get a good identification of the soft X-ray spectral features and determine the physical properties of the absorbing gas, we have made use of the PHASE (PHotoionised Absorption Spectral Engine) photoionization code (Krongold et al. 2003). The parameters that are usually let free are the ionization parameter of the gas, the equivalent hydrogen column density and the outflow velocity. Another parameter is the internal microturbulent velocity of the gas, which is very difficult to constrain because single absorption lines in the spectrum are unresolved by the actual available instruments and most of the observed features are blends of several transitions. Therefore we have fixed this velocity to 300 km s^{-1}, the same value used by Krongold et al. (2003) and Kaspi et al. (2001) to fit the spectra of NGC 3783. We note, however, that the exact value of this parameter has little effect on the results (see Krongold et al. 2009). The ionization parameter is defined as the ratio between the density of ionizing photons and the density of hydrogen particles, $U = Q(H)/4\pi cr^2 n_{\rm H}$, where r is the distance to the source, $n_{\rm H}$ is the hydrogen number density, c the speed of light and $Q(H)$ is the rate of hydrogen ionizing photons (or the integral over all hydrogen-ionizing photons of the ratio between the luminosity L_ν and the energy in the same frequency, $Q(H) = \int_{\nu=13.6{\rm eV}}^{\infty} L_\nu/h\nu\, {\rm d}\nu$).

The intrinsic SED of the source (Fig. 6) is used to calculate, with CLOUDY (version 08, Ferland et al. 1998), a grid of photoionization models to build the input table for PHASE. The optical-UV part of the SED is obtained from the OM data and for energies higher than ~0.1 keV we have used the EPIC-pn continuum model. In this way, the adopted SED represents the emission of UGC 11763 at the observation time. Only the photons with energies higher than ~0.1 keV will affect the absorption in the X-ray spectral range (Kaspi et al. 2001; Krongold et al. 2003). Nevertheless, the optical-UV part of the SED is important when we calculate the thermal equilibrium curve discussed in Sect. 6 below.

The fits with PHASE confirm the presence of warm material absorbing the source X-ray emission. Model $\mathcal{B}$ is the same as $\mathcal{A}$ but including one PHASE component. The result of the fitting using model $\mathcal{B}$ (Table 6) indicates that the absorbing gas is ionized ($T = 1.9 \pm 0.3 \times 10^5$ K), with an ionization parameter log $U = 1.7^{+0.4}_{-0.1}$ and has a moderate column density log $N_{\rm H} = 21.0 \pm 0.2$ cm^{-2} ($\chi^2_\nu = 0.97$, d.o.f. = 719). The F-test shows that, on the EPIC spectra, the fit with model $\mathcal{B}$ is better than with model $\mathcal{A}$ with a 99.9% of confidence level. The estimated value of the redshift of the absorbing material is 0.062 ± 0.001, to be compared to a measured optical redshift of 0.063 for UGC 11763 (Sect. 1). This, therefore may indicate that the material is flowing out from the nucleus with a velocity of about 300 ± 300 km s^{-1}, but it is also compatible with material at rest relative to the nucleus.

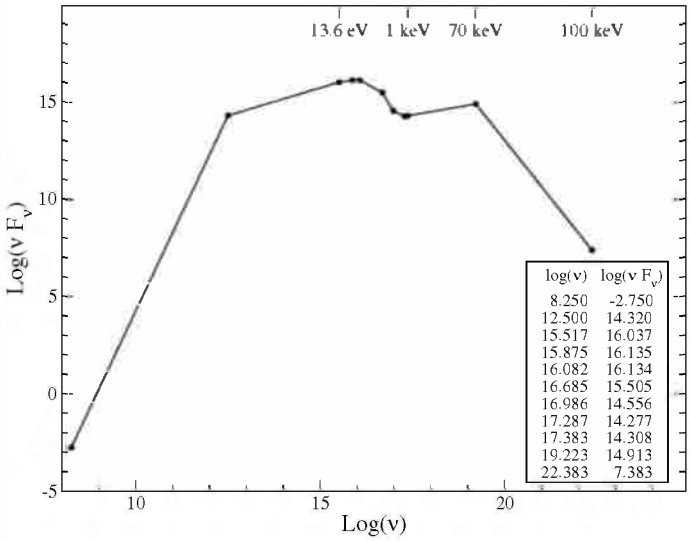

Fig. 6. Spectral energy distribution adopted for UGC 11763. Values in the optical-UV are estimated using the OM data and for energies higher than ~0.1 keV we have used the EPIC-pn continuum model.

The RGS2 residuals (at about 11–12 Å) suggest the existence of a second absorber. Therefore we have considered a new model with two absorbers (Model C, Table 6). The F-test shows that the fit with two warm absorbers is better than the fit with only one absorber at 99.9% confidence level. The second absorption component is compatible with it being highly ionized gas, (log $U = 2.6 \pm 0.1$ and $T = 1.2 \pm 0.1 \times 10^6$ K) with a column density log $N_{\rm H} = 21.51 \pm 0.01$ cm^{-2}. The inclusion of this component modified the parameters of the other model components: Γ, $K_{\rm pwlw}$ and kT are slightly higher than in Model $\mathcal{B}$, and the U and $N_{\rm H}$ of the first absorption component are lower and higher respectively (Table 6). There is also a change in the velocity of the low ionization absorbing component. For the Model $\mathcal{B}$ the velocity is compatible with material flowing out or being at rest with the nucleus, but for the Model C both absorbing components have velocities that are compatible with material flowing into the nucleus.

Besides the absorption features, there are also emission signatures on the high resolution spectra. Narrow emission lines of OVIII-Lyα, OVII-Heα and NeIX-Heα, among others, are frequently found in similar objects (e.g. Kaspi et al. 2000; Turner et al. 2003; Blustin et al. 2003; Pounds et al. 2004; Longinotti et al. 2008), hence, we have included in our model the emission

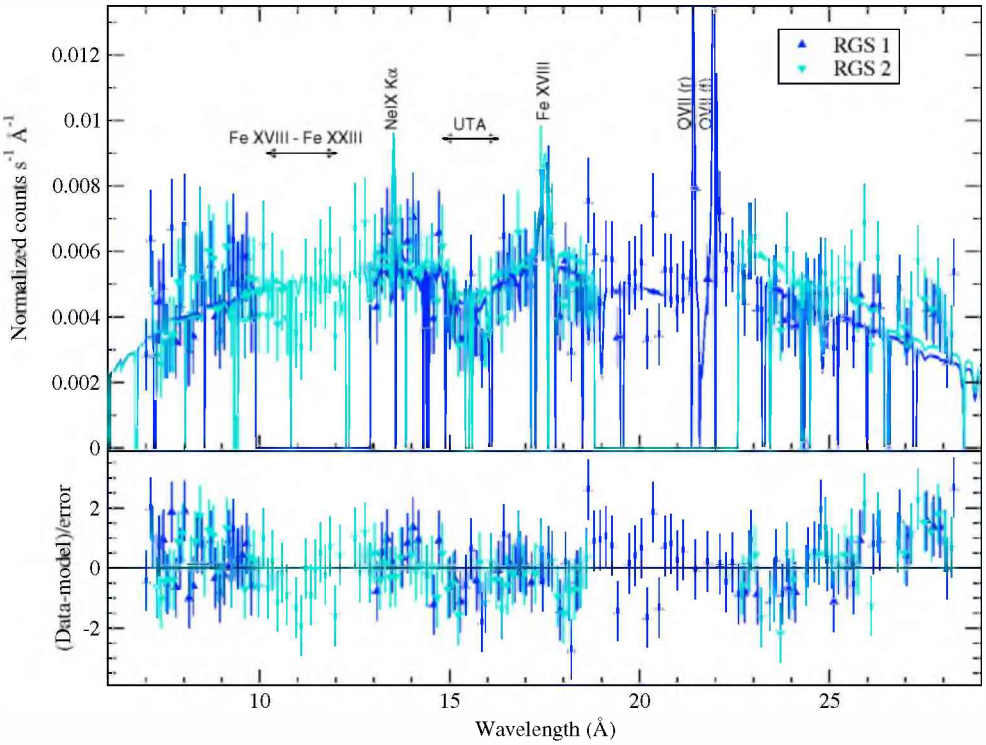

Fig. 7. High resolution X-ray spectra -in the rest frame- of UGC 11763 as obtained with RGS1, (blue up triangles), and RGS2 (cyan down triangles), and binned to 15 channels per bin. Solid lines are the convolution of the best fit model with instrument responses. (Model *C*.)

features as Gaussian line profiles. The procedure that has been followed is described below.

The lines are added on a one-by-one basis to check their statistical significance, constraining their energies to vary in a small range around their laboratory energies ($E_{\rm lab}$) and taking into account the redshift of the source. Since we cannot use only the F-test as a reliable criteria to compute the statistical significance of a Gaussian line (Protassov et al. 2002), we use a combined method to decide whether to include or not a line in our final model. Along with the F-test we check carefully the fit and the residuals, and finally we also take into account the wavelength positioning of the line.

We first include in the model the OVII-Heα lines triplet. The intercombination line is not found in the fitting process so we take it off and keep only the recombination (r) and forbidden (f) lines. The width of these lines takes a very small value (less than 10^{-5} keV) so we have fixed them to zero, i.e. to the instrumental resolution. In this way we find that the r and f lines of the OVII-Heα triplet are statistically significant for the fit (probability of 97%). These oxygen lines lie in the range of energies where no RGS2 data are available due to its non operational CCD, and where there are also bad pixels in the RGS1 spectrum. Therefore, their parameters are not well constrained (see Fig. 7 and Table 7). Nevertheless we consider that they are significant to the fit.

The next line added is OVIII-Lyα. This line turns out to be only marginally significant to the fit (probability of 86%), and its parameters are not well constrained either. Moreover, it lies just at the border of the non-operational CCD of the RGS2 instrument. Therefore we do not keep this line in our final model. To investigate its possible presence on the UGC 11763 spectra a longer observation is needed.

The emission signature seen at 17–18 Å has been modelled with a Gaussian line with its central energy varying between 0.62 and 0.73 keV (17–20 Å). The fitting process found that it is broad (σ about 1700 km s^{-1}) and statistically significant (probability of 98%). This line could correspond to FeXVIII at λ 17.62 Å. The NeIX-Heα triplet lines lay in the 13–14 A range. We have added them to the model finding that only one line is clearly detected and statistically significant (probability of 98%). This line could be a blend of the three components.

Table 7. Model *C* parameters for the narrow emission lines.

Line	$E_{\rm lab}$	$E_{\rm rest}$	$\lambda_{\rm rest}$	σ	$K_{\rm line}$
OVII (f)	0.5610	$0.564^{(a)}$	$21.97^{(a)}$	0 (frozen)	16^{+14}_{-14}
OVII (r)	0.5740	$0.579^{(a)}$	$21.41^{(a)}$	0 (frozen)	5^{+3}_{-3}
FeXVIII	0.7035	$0.708^{+0.005}_{-0.004}$	$17.50^{+0.11}_{-0.09}$	$0.004^{+0.004}_{-(a)}$	3^{+1}_{-3}
NeIX Kα	blend	$0.917^{+0.007}_{-0.015}$	$13.52^{+0.10}_{-0.22}$	$0.0001^{(a)}$	2^{+2}_{-1}

$E_{\rm lab}$ is the laboratory energy of the lines. $E_{\rm rest}$ and $\lambda_{\rm rest}$ are the energy and wavelength of the lines given in the rest frame of the object. $E_{\rm lab}$, $E_{\rm rest}$ and σ are given in keV, λ in Å and $K_{\rm line}$ in 10^{-5} ph cm^{-2} s^{-1}. $^{(a)}$ Unconstrained parameter, see text. Errors quoted are at 90% confidence level.

The parameter values of the best fit model (Model *C*) are summarized in Tables 6 and 7. This model and its errors are plotted in Figs. 7 and 8.

6. Discussion

From the OM data of UGC 11763 we have found that the IUE spectra is representative of its flux state during the *XMM-Newton* observation. Using the IUE flux at 2500 Å and the flux at 2 keV from EPIC-pn data, $F(2\,{\rm keV}) = 7{\times}10^{-13}$ erg s^{-1} cm^{-2} keV^{-1}, we obtain an optical/X-ray spectral index $\alpha_{ox} = 1.6$ for this object. This value is similar to those given by Wilkes & Elvis (1987)

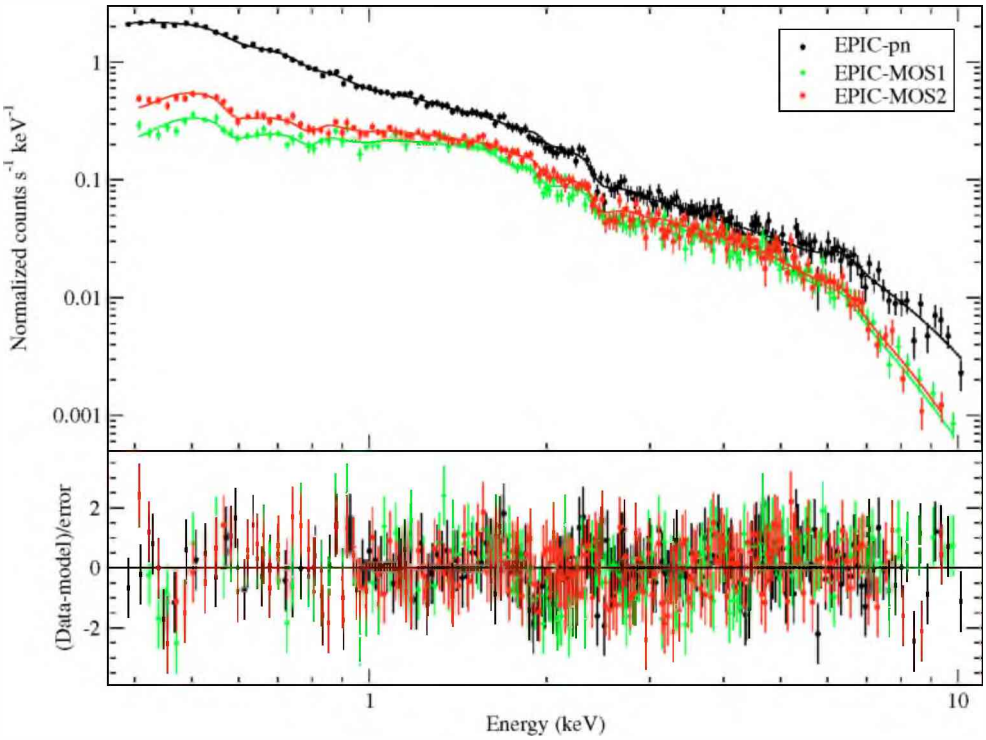

Fig. 8. Low resolution X-ray spectra – in the rest frame – of UGC 11763 as obtained with the EPIC-pn (black dots), EPIC-MOS1 (green diamonds) and EPIC-MOS2 (red squares) cameras. The best fit model (Model *C*) convolved with the instrument response of each camera is shown in solid line.

and Gallo (2006) and is typical of Seyfert 1 AGNs as shown by these authors.

Regarding the shape of the continuum emission from the AGN, a power law accounts for the hard X-rays. It has a standard spectral index for Seyfert 1 galaxies or AGNs (Piconcelli et al. 2005) and is in good agreement with the values found by Inoue et al. (2007) from the same *XMM-Newton* observation and by Singh et al. (1991) from *EXOSAT Observatory* data taken with the low-energy and medium-energy detectors and the source in a low luminosity state.

The EPIC data show the possible presence of the Fe Kα line around 6 keV. The line parameters are unconstrained (as seen by the large error bars); in addition, the line is weak (equivalent width of $0.23^{+0.15}_{-0.11}$ keV) and rather broad (σ = $16\,000^{+15\,000}_{-7\,000}$ km s^{-1}). Therefore we consider the significance of this line to be very low. It is interesting to note that Inoue et al. (2007) also included the Fe Kα line in their final model, at a similar energy within the errors. Its reported width is smaller than found here, but their larger σ error makes their value and ours compatible.

The extrapolation of the hard-X-ray model to lower energies, down to 0.35 keV, reveals the existence of a large soft-X-ray flux in excess of the hard power law, from ~0.9 keV and below. This excess has also been reported by Masnou et al. (1992) from *Einstein Observatory* IPC (Imaging Proportional Counter) data and Singh et al. (1991) from *EXOSAT Observatory* data. After testing the most typical components used to model the soft excess we find that it can be accounted for by a black body component with $kT \sim 0.1$ keV (consistent with the value obtained by Inoue et al. 2007) as found in many other Seyfert galaxies (Piconcelli et al. 2005).

In fact, we find that the continuum spectral characteristics of UGC 11763 are typical of Seyfert 1 galaxies. UGC 11763 shows soft X-ray excess emission as detected in several Seyfert 1 and NLS1 objects (Boller et al. 1996; Piconcelli et al. 2004). Regarding variability: in the long term (several years) variations by a factor of about 10 have been detected; in the short term, variations by about 1.5 have been detected in our 37 ks observation. This behavior is typical of "normal" Seyfert 1s (e.g., Markowitz 2005; Winter et al. 2008; Dewangan et al. 2008). The rapid and large-amplitude variability as seen in other NLS1s (Boller 2000) is not detected during our observation. For example, for the NLS1 NGC 4051, McHardy et al. (1995) reported a flux variation by a factor of about 10 during a 28 ks *ROSAT* observation. However, as can be seen in the middle right panel of Fig. 1 of Smith & Vaughan (2007), NGC 4051 has also periods during which no large-amplitude variability is observed. The X-ray properties of UGC 11763 do not show the extreme properties of other NLS1 in X-rays. Moreover, Gallo (2006) suggests that NLS1s show complex spectra while at a low flux state. We caught UGC 11763 at a flux about 10 times lower than in other epochs. Still none of the complex spectral properties attributed by Gallo to NLS1s in low state have been detected. We therefore conclude that UGC 11763 is probably a NLS1 at the border between the NLS1 and Seyfert 1 classification. Its optical properties suggest a NLS1 but there is no conclusive prove of this nature from the present X-ray observations.

Our simultaneous analysis of the EPIC and RGS data reveals the presence of absorption by ionized gas in the line of sight to UGC 11763. Two absorbing components are clearly required to fit the data (see Table 6) as has already been found for many other objects that show the presence of warm absorbers (e.g., IRAS 13349+2438, Sako et al. 2001; NGC 7469, Blustin et al. 2003; NGC 3783, Krongold et al. 2003; Mrk 279, Costantini et al. 2007; NGC 985, Krongold et al. 2009). A low ionization component (LIC) – $\log U = 1.65^{+0.07}_{-0.08}$, $N_{\rm H} = 1.6 \pm 0.9 \times 10^{21}$ cm^{-2}

($T = 1.8 \pm 0.2 \times 10^5$ K) –, gives rise to absorption by the Fe M-shell UTA (charge states XII to XVI). A high ionization component (HIC) – $\log U = 2.6 \pm 0.1$, $N_{\rm H} = 3.2 \pm 0.1 \times 10^{21}$ cm^{-2}, twice higher than for the LIC, ($T = 1.2 \pm 0.1 \times 10^6$ K) – produces absorption by FeXX-FeXXV. The velocity of both components relative to the systemic velocity of UGC 11763 is consistent with a single value of 500 ± 300 km s^{-1}.

After the inclusion of the second absorber, residuals at 11 Å on the RGS2 data (Fig. 7) were still found that are consistent with an absorption feature by FeXXIII. This led us to test the presence of a third absorption component. The inclusion of this component in the model, however, does not improve the fit. This result does not rule out the existence of a third absorbing component in the line of sight to this source, but data with a higher signal-to-noise ratio are required in order to establish or discard its presence.

Different scenarios have been suggested to model the observed complexity of the absorbing material in AGNs. Krongold et al. (2003, 2005, 2009) and Netzer et al. (2003) modelled the absorption with a discrete number of absorbing components finding that these components appear to be in pressure balance with each other. With a different idea, Steenbrugge et al. (2003, 2005) and Ogle et al. (2004) suggested that the absorption could be produced by a radial distribution of material with a continuous distribution of temperatures. However, recent models have shown that models consisting in discrete phases in pressure balance can also model the ionized absorbers in these objects (Krongold et al. 2007, for NGC 4051; and Chelouche 2009, for NGC 5548). Alternatively, it has also been suggested that, rather than a multi-phase medium in pressure balance, the absorber could be a single system with a constant total (gas plus radiation) pressure with a stratified distribution in temperature (Różańska et al. 2006; Gonçalves et al. 2006).

As pointed out by Krongold et al. (2003) a wide well resolved UTA feature sets tight restrictions on the ionization degree of the absorbing material and different values of the ionization parameter lead to different shapes and wavelength ranges for the UTA. Figure 7 shows a well defined UTA feature in the RSGs spectra of UGC 11763. A medium with a smooth distribution of temperatures is unlikely to produce this well defined feature (for a detailed discussion see Krongold et al. 2003).

Our model presents a simple picture: two kinematically indistinguishable gas components with rather different photoionization equilibrium temperatures and two widely separated ionization parameter values. This simple picture suggests that the absorption observed in the source spectrum may arise from two phases of the same medium. To test the possibility of having a multi-phase medium in pressure equilibrium we have calculated the thermal equilibrium curve $\log(T)$ vs. $\log(U/T)$ (hereafter S-curve) for UGC 11763 (Fig. 9) using the SED described in Sect. 5.2. The S-curve represents the points where heating and cooling processes are in equilibrium. The $\log(U/T)$ value is inversely proportional to the gas pressure, so that vertical lines in the plot indicate isobaric conditions. More than one phase may exist at pressures where the S-curve is multivalued (Krolik & Kriss 2001; Chakravorty et al. 2009). Regions of the curve with negative slope are unstable because any isobaric perturbation will produce net heating or cooling in the gas, see Krongold et al. (2005) for further details. For this object we find that the LIC and HIC components lie in stable parts of the curve (Fig. 9). Both components are consistent with having roughly the same gas pressure. This fact and the similar velocity (see Table 6) we find for both absorbers suggest that the two components in UGC 11763 could indeed constitute a multi-phase medium.

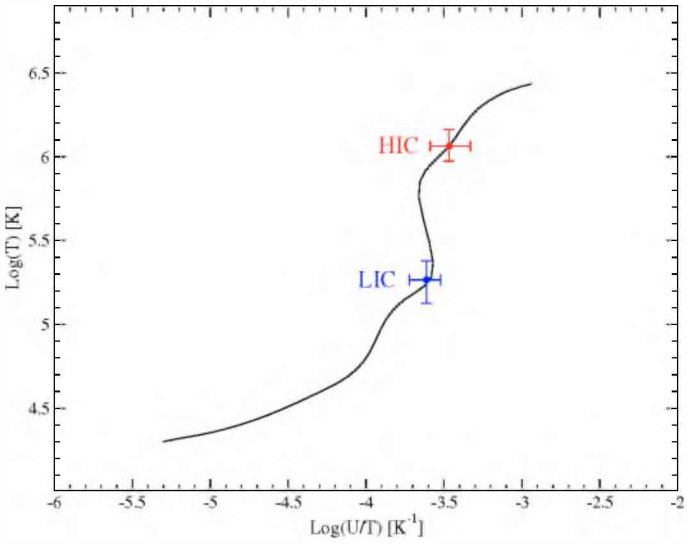

Fig. 9. Thermal stability curve of UGC 11763 obtained using the SED based on the simultaneous multiwavelength data obtained in this observation and assuming a column density of $\log N_{\rm H} = 21.5$ cm^{-1}. We have indicated the position of the two components of photoionized absorbing material from model *C*.

In this sense, it is noteworthy that the LIC has a relatively high temperature ($T = 1.8 \pm 0.2 \times 10^5$ K). Given the shape of the S-curve, only gas at such temperature could coexist in pressure equilibrium with the high ionization HIC component. In fact, the UTA in this object is formed by FeXII-FeXVI; this is striking since UTAs found in warm absorbers in other Seyfert 1 galaxies are colder ($T \sim$ few $\times 10^4$ K) and are produced by FeVII-FeXII (see Krongold et al. 2009, and references therein) and in those objects such charge states are the ones required for pressure equilibrium between their absorbing components (for them, the gas producing FeXIII-FeXVI lies on unstable regions of the S-curve).

As we have mentioned in Sect. 1, the same AGNs that show absorption lines in the UV also show signatures of X-ray absorbers (Mathur et al. 1995; Crenshaw et al. 1999; Kriss 2002). In many cases, the absorbers show similar outflow velocities and similar ionization states in the UV and X-rays, and in this cases, it is straightforward to assume that the same media is producing absorption in both bands (e.g. Arav et al. 2007). Nevertheless, since this is not the case for all the objects studied, the precise relation between the absorbers in both bands is still uncertain. Crenshaw et al. (1999) and Dunn et al. (2007, 2008) have studied the UV spectrum of UGC 11763. Crenshaw et al. found signatures of two absorbing components in the lines due to CIV, NV, and OVI with radial velocities of -1568 ± 39 and $+45 \pm 41$ km s^{-1}. Later, Dunn et al. also found two components in the lines due to OVI($\lambda\lambda$ 1032, 1038) with radial velocities similar to those found by Crenshaw et al.. However, these reported velocities do not agree with the ones we find for the X-ray absorber. Moreover, the ionization states we find in the LIC and HIC components are too high for OVI to produce detectable absorption features in the UV (see for example Arav et al. 2007). This implies that the systems producing the absorption in X-rays are not the same as those producing absorptions in the UV.

We find four statistically significant emission lines (see Fig. 10). Three of them can be identified as OVII Heα(r), OVII Heα(f) and a blend of the NeIX Heα triplet. The energies of the lines are slightly different from their laboratory values.

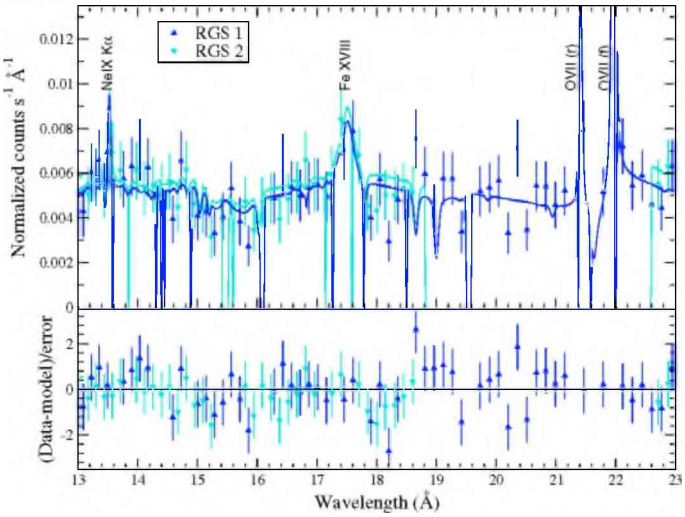

Fig. 10. Enlargement of Fig. 7 showing the fitted lines.

Nevertheless, taking into account the errors in the energy determination of the lines during the fitting process, their positions are consistent with the rest frame of UGC 11763. These lines are often found in other Seyfert 1 and NLS1 AGNs as NGC 3783 (Kaspi et al. 2000), NGC 3516 (Turner et al. 2003), NGC 4051 (Pounds et al. 2004) and Mrk 335 (Longinotti et al. 2008) among others. The fourth line can be identified as the FeXVIII line at 17.62 Å, also detected in the spectra of NGC 7469 by Blustin et al. (2007). None of these lines are resolved in the spectra, which does not allow the reliable determination of their widths. Therefore, it is possible that all of them arise in the same medium.

As a final remark we would like to point out that both warm absorbing components appear to be redshifted ($z = 0.0647 \pm 0.0009$) with respect to the emission lines and the rest frame of the object. This could be indicating the presence of an inflow. However, given the loss in spectral resolution we have to assume in order to increase the signal-to-noise of our spectra, the quality of the data is not sufficient to constrain the velocity of these components. While the presence of infalling ionized gas could have important potential effects for our understanding of AGN winds, the present measurements are not conclusive. A longer observation of this source is needed to further study this possibility, as well as to constrain the physical parameters of the emitting media.

7. Summary and conclusions

We have analyzed all the data of UGC 11763 taken by the *XMM-Newton* satellite. Joining the optical-UV information with the X-ray information we have built the SED of this object at the epoch of observation. We have concentrated our efforts mainly on the analysis of the X-ray spectra, finding that the continuum emission of the source can be characterized by a power law and a black body components. The continuum emission is absorbed by ionized material in the line of sight to the source. We have found two absorbing components that are consistent with their being in pressure equilibrium, indicating that they could constitute two phases of the same medium. This idea is supported by an UTA of higher ionization than those found in other AGNs. Furthermore, we have found some emission lines, among them an unusual FeXVIII emission line. The X-ray properties of UGC 11763 described here are compatible with it being either a normal Seyfert 1 galaxy or a NLS1. There is no sign of the extreme X-ray properties, like large amplitude short-term variability or spectral complexity, detected in other NLS1 at least at some epochs. More data are needed in order to get a full characterization of this object.

Acknowledgements. We are grateful to the referee, Elisa Costantini, for a careful revision of this manuscript that greatly improved its clarity. This research is completely based on observations obtained with *XMM-Newton*, an ESA science mission with instruments and contributions directly funded by ESA Member States and NASA. For the spectral fitting use of software provided by the Chandra X-ray Centre (CXC) in the application package Sherpa has been made. This work has been supported by DGICYT grants AYA-2004-02860-C03 and AYA2007-67965-C03-03. G.H. and M.C. acknowledge support from the Spanish MEC through FPU grants AP2003-1821 and AP2004-0977. Furthermore, partial support from the Comunidad de Madrid under grants S-0505/ESP/000237 (ASTROCAM) and S-0505/ESP-0361 (ASTRID) is acknowledged. M.C. and G.H. also thank the hospitality of the UNAM. Y.K. acknowledges support from the Faculty of the European Space Astronomy Centre (ESAC), and the hospitality of ESAC.

References

Arav, N., Gabel, J. R., Korista, K. T., et al. 2007, ApJ, 658, 829
Blustin, A. J., Branduardi-Raymont, G., Behar, E., et al. 2003, A&A, 403, 481
Blustin, A. J., Kriss, G. A., Holczer, T., et al. 2007, A&A, 466, 107
Boller, T. 2000, New Astron. Rev., 44, 387
Boller, T., Brandt, W. N., & Fink, H. 1996, A&A, 305, 53
Boroson, T. A. 2002, ApJ, 565, 78
Boroson, T. A., & Green, R. F. 1992, ApJS, 80, 109
Brandt, W. N., Mathur, S., & Elvis, M. 1997, MNRAS, 285, L25
Chakravorty, S., Kembhavi, A. K., Elvis, M., & Ferland, G. 2009, MNRAS, 393, 83
Chelouche, D. 2009, ApJ, 692, 375
Clements, E. D. 1981, MNRAS, 197, 829
Constantin, A., & Shields, J. C. 2003, PASP, 115, 592
Costantini, E., Kaastra, J. S., Arav, N., et al. 2007, A&A, 461, 121
Crenshaw, D. M., Kraemer, S. B., Boggess, A., et al. 1999, ApJ, 516, 750
de Bruyn, A. G., & Sargent, W. L. W. 1978, AJ, 83, 1257
den Herder, J. W., Brinkman, A. C., Kahn, S. M., et al. 2001, A&A, 365, L7
Dewangan, G. C., Mathur, S., Griffiths, R. E., & Rao, A. R. 2008, ApJ, 689, 762
Dickey, J. M., & Lockman, F. J. 1990, ARA&A, 28, 215
Dunn, J. P., Crenshaw, D. M., Kraemer, S. B., & Gabel, J. R. 2007, AJ, 134, 1061
Dunn, J. P., Crenshaw, D. M., Kraemer, S. B., & Trippe, M. L. 2008, AJ, 136, 1201
Ferland, G. J., Korista, K. T., Verner, D. A., et al. 1998, PASP, 110, 761
Freeman, P., Doe, S., & Siemiginowska, A. 2001, in SPIE Conf. Ser., 4477, ed. J.-L. Starck, & F. D. Murtagh, 76
Gabel, J. R., Crenshaw, D. M., Kraemer, S. B., et al. 2003, ApJ, 583, 178
Gallo, L. C. 2006, MNRAS, 368, 479
Gehrels, N. 1986, ApJ, 303, 336
George, I. M., Turner, T. J., Netzer, H., et al. 1998, ApJS, 114, 73
Ghosh, K. K., Swartz, D. A., Tennant, A. F., Wu, K., & Ramsey, B. D. 2004, ApJ, 607, L111
Gonçalves, A. C., Collin, S., Dumont, A.-M., et al. 2006, A&A, 451, L23
Greene, J. E., & Ho, L. C. 2005, ApJ, 630, 122
Grier, C. J., Peterson, B. M., Bentz, M. C., et al. 2008, ApJ, 688, 837
Grupe, D., & Mathur, S. 2004, ApJ, 606, L41
Grupe, D., Wills, B. J., Leighly, K. M., & Meusinger, H. 2004, AJ, 127, 156
Halpern, J. P. 1982, Ph.D. Thesis, AA, Harvard Univ., Cambridge, MA
Ho, L. C., Darling, J., & Greene, J. E. 2008, ApJS, 177, 103
Huchra, J. P., Vogeley, M. S., & Geller, M. J. 1999, ApJS, 121, 287
Inoue, H., Terashima, Y., & Ho, L. C. 2007, ApJ, 662, 860
Jansen, F., Lumb, D., Altieri, B., et al. 2001, A&A, 365, L1
Kaspi, S., Brandt, W. N., Netzer, H., et al. 2000, ApJ, 535, L17
Kaspi, S., Brandt, W. N., Netzer, H., et al. 2001, ApJ, 554, 216
Komossa, S. 2000, New Astron. Rev., 44, 483
Kriss, G. A. 2002, in Mass Outflow in Active Galactic Nuclei: New Perspectives, ed. D. M. Crenshaw, S. B. Kraemer, & I. M. George, ASP Conf. Ser., 255, 69
Kriss, G. A., Blustin, A., Branduardi-Raymont, G., et al. 2003, A&A, 403, 473

Kriss, G. A., Green, R. F., Brotherton, M., et al. 2000, ApJ, 538, L17
Krolik, J. H., & Kriss, G. A. 2001, ApJ, 561, 684
Krongold, Y., Nicastro, F., Brickhouse, N. S., et al. 2003, ApJ, 597, 832
Krongold, Y., Nicastro, F., Elvis, M., et al. 2005, ApJ, 620, 165
Krongold, Y., Nicastro, F., Elvis, M., et al. 2007, ApJ, 659, 1022
Krongold, Y., Jiménez-Bailón, E., Santos-Lleo, M., et al. 2009, ApJ, 690, 773
Lawson, A. J., & Turner, M. J. L. 1997, MNRAS, 288, 920
Longinotti, A. L., Nucita, A., Santos-Lleo, M., & Guainazzi, M. 2008, A&A, 484, 311
Markowitz, A. 2005, ApJ, 635, 180
Masnou, J. L., Wilkes, B. J., Elvis, M., McDowell, J. C., & Arnaud, K. A. 1992, A&A, 253, 35
Mason, K. O., Breeveld, A., Much, R., et al. 2001, A&A, 365, L36
Mathur, S., Elvis, M., & Wilkes, B. 1995, ApJ, 452, 230
Mathur, S., Wilkes, B., Elvis, M., & Fiore, F. 1994, ApJ, 434, 493
McHardy, I. M., Green, A. R., Done, C., et al. 1995, MNRAS, 273, 549
Mullaney, J. R., & Ward, M. J. 2008, MNRAS, 385, 53
Netzer, H., Kaspi, S., Behar, E., et al. 2003, ApJ, 599, 933
Ogle, P. M., Mason, K. O., Page, M. J., et al. 2004, ApJ, 606, 151
Osterbrock, D. E., & Pogge, R. W. 1985, ApJ, 297, 166
Peterson, B. M., Ferrarese, L., Gilbert, K. M., et al. 2004, ApJ, 613, 682
Piconcelli, E., Jimenez-Bailón, E., Guainazzi, M., et al. 2004, MNRAS, 351, 161
Piconcelli, E., Jimenez-Bailón, E., Guainazzi, M., et al. 2005, A&A, 432, 15
Pounds, K. A., Reeves, J. N., King, A. R., & Page, K. L. 2004, MNRAS, 350, 10
Protassov, R., van Dyk, D. A., Connors, A., Kashyap, V. L., & Siemiginowska, A. 2002, ApJ, 571, 545
Reynolds, C. S. 1997, MNRAS, 286, 513
Rózańska, A., Goosmann, R., Dumont, A.-M., & Czerny, B. 2006, A&A, 452, 1
Sako, M., Kahn, S. M., Behar, E., et al. 2001, A&A, 365, L168
Saxton, R. D., Read, A. M., Esquej, P., et al. 2008, A&A, 480, 611
Singh, K. P., Rao, A. R., & Vahia, M. N. 1991, ApJ, 372, 49
Smith, R., & Vaughan, S. 2007, MNRAS, 375, 1479
Steenbrugge, K. C., Kaastra, J. S., de Vries, C. P., & Edelson, R. 2003, A&A, 402, 477
Steenbrugge, K. C., Kaastra, J. S., Crenshaw, D. M., et al. 2005, A&A, 434, 569
Steenbrugge, K. C., Fenovčík, M., Kaastra, J. S., Costantini, E., & Verbunt, F. 2009, A&A, 496, 107
Tananbaum, H., Avni, Y., Branduardi, G., et al. 1979, ApJ, 234, L9
Turner, M. J. L., Abbey, A., Arnaud, M., et al. 2001, A&A, 365, L27
Turner, T. J., Kraemer, S. B., Mushotzky, R. F., George, I. M., & Gabel, J. R. 2003, ApJ, 594, 128
Véron-Cetty, M.-P., & Véron, P. 2006, A&A, 455, 773
Voges, W., Aschenbach, B., Boller, T., et al. 1999, A&A, 349, 389
Wakker, B. P., Savage, B. D., Sembach, K. R., et al. 2003, ApJS, 146, 1
Wilkes, B. J., & Elvis, M. 1987, ApJ, 323, 243
Williams, O. R., Turner, M. J. L., Stewart, G. C., et al. 1992, ApJ, 389, 157
Winter, L. M., Mushotzky, R. F., Tueller, J., & Markwardt, C. 2008, ApJ, 674, 686